Structural and magnetic properties of Co_2MnSi thin films

M. Belmeguenai[*,1], F. Zighem[1,2], D. Faurie[1], H. Tuzcuoglu[1], S.-M. Chérif[1], P. Moch[1], K. Westerholt[3], and W. Seiler[4]

[1] LSPM, Institut Galilée, UPR 3407 CNRS, Université Paris 13, 99 Av. Jean-Baptiste Clément, 93430 Villetaneuse, France
[2] IMCN, Université Catholique de Louvain, Place Croix du Sud 1, 1348 Louvain-la-Neuve, Belgium
[3] Institut für Experimentalphysik/Festkörperphysik, Ruhr-Universität Bochum, 44780 Bochum, Germany
[4] PIMM, ENSAM, 151 Boulevard de l'Hôpital, 75013 Paris, France

Keywords ferromagnetic resonance, Heusler alloys, magnetic anisotropy, spin waves

*

Co_2MnSi (CMS) films of different thicknesses (20, 50, and 100 nm) were grown by radio frequency (RF) sputtering on a-plane sapphire substrates. Our X-rays diffraction (XRD) study shows that, in all the samples, the cubic ⟨110⟩ CMS axis is normal to the substrate and that six well defined preferential in-plane orientations are present. Static and dynamic magnetic properties were investigated using vibrating sample magnetometry (VSM) and microstrip line ferromagnetic resonance (MS-FMR), respectively. From the resonance measurements *versus* the direction and the amplitude of an applied magnetic field, most of the magnetic parameters are derived, i.e.: the magnetization, the gyromagnetic factor, the exchange stiffness coefficient, and the magnetic anisotropy terms. The in-plane anisotropy results from the superposition of two terms showing a twofold and a fourfold symmetry, respectively. The observed behavior of the hysteresis loops is in agreement with this complex form of the in-plane anisotropy.

1 Introduction Due to their strong spin polarization at the Fermi level and to their rather high Curie temperature the full Heusler alloys are interesting candidates for various applications. For instance, the Co_2MnSi (CMS) full Heusler alloy, which has a Curie temperature of 985 K [1, 2], was recently inserted in spintronics devices consisting in magnetic tunnel junctions (MTJs) containing one or two CMS electrodes and various barriers [3–8]. Some Heusler alloys were used as MTJ electrodes with an amorphous Al-oxide barrier [9–12], allowing for a tunnel magnetoresistance (TMR) ratio of 159% at 2 K in a CMS/Al–O/CoFe structure [6]. A large TMR ratio, up to 753% at 2 K and to 217% at room temperature, was obtained with CMS used in TMJs with MgO barriers [13].

Due to the attractive potential of CMS for spintronics applications, particularly in order to produce magnetic random access memories (MRAMs), its dynamic behavior within the 1–10 GHz frequency range, which, in this technology, is a key in view of increasing data rates in magnetic storage devices, is actively studied [14–17]. However these studies are mainly focused on CMS thin films grown on MgO or GaAs substrates which provide a less complicated crystal texture than the Al_2O_3 substrates. In this latter case the relationship between the magnetic anisotropy and the crystal structure of the film plays an important role. This was pointed out in our previously published work concerning a parent compound, Co_2MnGe [18, 19]. The replacement of Ge by Si, in films intentionally elaborated under identical conditions, is expected to give rise to similar conclusions, as confirmed in the following paper.

We then investigate the static and dynamic magnetic properties of CMS films grown on *a*-plane sapphire substrate. We attempt to find a correlation between their structure, their thickness, and their magnetic anisotropies. In addition, we focus on the experimental evaluation of the exchange stiffness constant A_{ex}, in CMS films, which is an important parameter from both fundamental and application points of view. Ferromagnetic resonance in microstrip line (MS-FMR) with an in-plane and out-of-plane perpendicular applied magnetic field and sample vibrating magnetometry were used in this experimental study. The (MS-FMR) technique provides information about various important properties, such as the

values of the effective magnetization, of the Landé factor g, of the effective magnetic anisotropy fields and of the exchange stiffness constant.

The paper is organized as follows: in Section 2 we briefly present the preparation of the samples and their structural properties investigated by X-rays diffraction (XRD). Section 3.1 exposes their main static magnetic characteristics derived from our vibrating sample magnetometry (VSM) measurements. Section 3.2 presents and discusses our dynamic measurements performed with the help of MS-FMR and we conclude that the relation between structural and magnetic properties cannot be established. In Section 4, conclusions are drawn: the rather complex texture of the films on a-sapphire substrates, which involves six distinct in-plane orientations, does not vary from sample to sample; however the in-plane magnetic anisotropy terms are sample dependent and their correlation with the film thickness cannot be established. Therefore, their magnetic properties cannot be tuned rigorously and, consequently, it is more convenient to use III–V semiconductor and MgO substrates for high-quality spintronic devices where well defined magnetic properties are required.

2 Sample preparation and structural properties

The CMS thin films (20, 50, and 100 nm in thickness) were deposited on a-plane sapphire substrates by UHV-magnetron rf-sputtering using pure Ar at a pressure of 5×10^{-3} mbar as sputter gas. The growth conditions (growth rate, Ar pressure, and substrate temperature) were preliminarily tested in order to optimize the structural quality of the films [20]. The found best parameters are: base pressure of 2×10^{-9} mbar in the sputtering system, sputtering rate of 0.03 nm/s for CMS and of 0.025 nm/s for the previously deposited vanadium seed underlayer. During the deposition the temperature of the substrates was kept constant at 470 °C. Heusler alloy targets with a diameter of 10 cm were cut from single phase stoichiometric ingots prepared by high frequency melting of the components in high purity graphite crucibles. The Al_2O_3 sapphire a-plane substrate was, as mentioned above, preliminarily covered with a 5 nm thick vanadium-seed-layer in order to induce a high quality (110) growth of the Heusler compound. After cooling them down to room temperature all the films were subsequently covered by a 5 nm thick gold layer protecting them against oxidation.

X-rays diffraction measurements were performed using a four-circle diffractometer in Bragg–Brentano geometry in order to obtain θ–2θ patterns and ϕ-scans, operating at 40 kV and 40 mA, and using a Cu X-rays source ($\lambda = 0.15418$ nm). In all the films, the θ–2θ pattern (Fig. 1a) indicates that a $\langle 110 \rangle$-type cubic axis is normal to the sample plane. The CMS deduced cubic lattice constant ($a = 5.658$ Å for the 100- and 50-nm-thick samples and $a = 5.639$ Å for 20-nm-thick film) is in good agreement with the previously published value (5.654 Å) [2]. The out-of-plane misfit of the periodic lattice parameter between the Heusler film and the underlying sapphire substrate overpasses 16%; the vanadium-seed layer, which shows the same (110) orientation, provides an out-of-plane V/Heusler misfit of only about 6.6%; assuming identical orientations of the cubic in-plane $\langle 001 \rangle$ axis in the Heusler and in the interlaying vanadium film, the in-plane V/Heusler misfit is also evaluated to 6.6%.

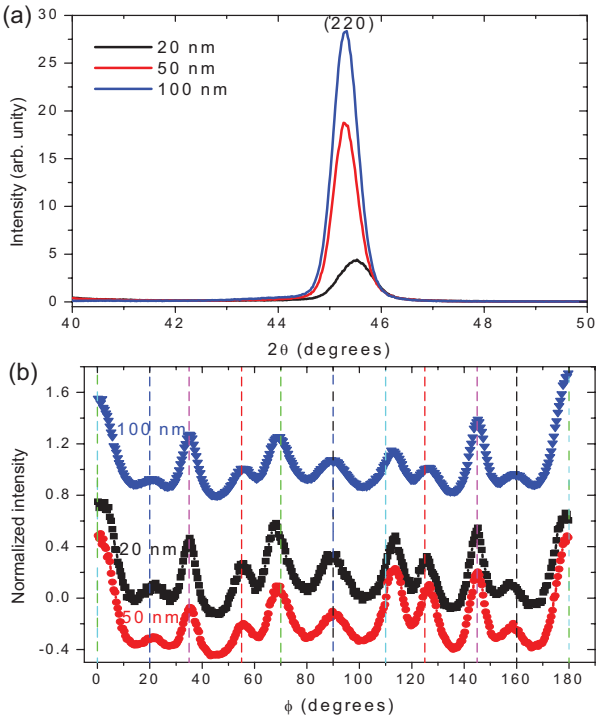

Figure 1 (online color at: www.pss-a.com) (a) X-rays θ–2θ scan using the Cu Kα_1 radiation and (b) angular variations ϕ-scan of the intensity around $\psi = 60°$ for different Co_2MnSi thin films. Graphs are shifted vertically with respect to that of the 20-nm-thick sample for clearness. The vertical color and dashed lines refer to the expected positions of the diffraction peak relative to the different variants belonging to the four observed families.

The samples behave as {110} fiber textures containing well defined zones showing significantly higher intensities, as shown in Fig. 1b, which represents ϕ-scans at $\psi = 60°$ (here, ψ is the declination angle between the scattering vector and the direction normal to the film, ϕ is the rotational angle around this direction). The regions related to the observed maxima correspond to orientation variants which can be grouped into four families. Two of them were observed in a previous study [18, 19] concerning thin films of a neighboring Heusler compound, Co_2MnGe, prepared using an identical protocol: in the first one the threefold $[1\bar{1}1]$ or $[1\bar{1}\,\bar{1}]$ axis is oriented along the c rhombohedral direction of the sapphire substrate, thus defining two kinds of distinct domains, respectively, characterized by their [001] axis inclined at $+54.5°$ or at $-54.5°$ with respect to this c orientation. The second family is rotated by 90° from the first one and also contains two variants. In addition, we observe a third family consisting in domains with their [001] axis along c and a fourth one with their [001] axis normal to c. This distribution into six kinds of domains does not appreciably

vary from sample to sample, as shown on Fig. 1b. This difference in the structure between the CMS and Co_2MnGe films probably arises from the variation of the lattice mismatch.

3 Magnetic properties

3.1 Static magnetic measurements For all the samples the hysteresis curves were studied at room temperature with an in-plane magnetic field H applied along various orientations, as shown in Fig. 2 (φ_H is the angle between H and the c-axis of the substrate). The variations of the reduced remanent magnetization (M_r/M_s) as function of φ_H are also depicted in Fig. 4, in view of comparison with other results discussed in the next section. For any given direction of the applied field the shape of the hysteresis loop

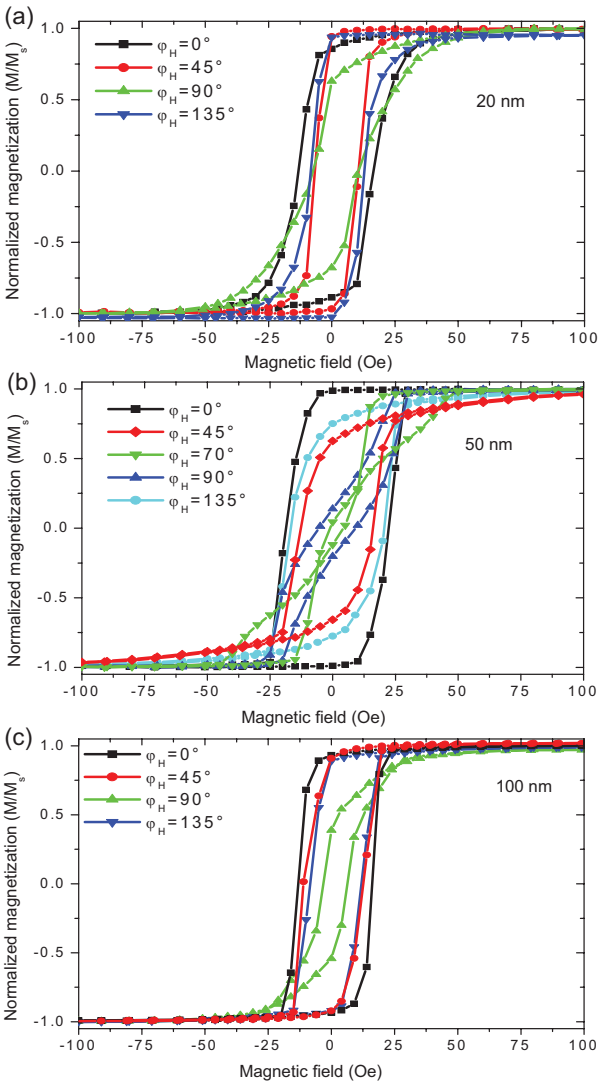

Figure 2 (online color at: www.pss-a.com) VSM magnetization loops of the (a) 20-nm-thick, (b) 50-nm-thick, and (c) 100-nm-thick Co_2MnSi samples. The magnetic field is applied parallel to the film surface, at various angles (φ_H) with the c-axis of the sapphire substrate.

is sample dependent, suggesting significant differences in the amplitudes and in the principal directions describing the in-plane anisotropy. Let us briefly discuss the case of the 50-nm film: as shown on Fig. 2b, when H lies along c ($\varphi_H = 0^\circ$) a typical easy axis square-shaped loop is observed, with a full normalized remanence ($M_r/M_s = 0.99$) and a coercive field of 20 Oe. As φ_H increases M_r/M_s decreases and the hysteresis curve tends to transform into a hard axis loop. When φ_H reaches 70° its shape becomes more complicated: it consists of three smaller loops. A further increase of φ_H restores an almost rectangular shape. Notice the observed difference between orthogonal directions (e.g., $\varphi_H = 45^\circ$ *vs.* $\varphi_H = 135^\circ$ or: $\varphi_H = 0^\circ$ *vs.* $\varphi_H = 90^\circ$) which prevents a simple interpretation based on a fourfold in-plane anisotropy. Our static (reduced remanent magnetization) and dynamic data qualitatively agree with a description of the in-plane anisotropy in terms of an addition of fourfold and twofold contributions with slightly misaligned easy axes for some samples (50-nm-thick film). This slight misalignment between the anisotropy axes is traduced by minima of the remanent magnetization occurring at angles different from 90° and 270° (Fig. 4c).

Figures 2a and c show a series of hysteresis loops related to the other films: here again, they qualitatively agree with the above description, but with different relative contributions and orientations of the twofold and of the fourfold anisotropy terms. At evidence, a quantitative estimation of the pertinent in-plane anisotropy terms monitoring the dynamic properties presented in the next section cannot be derived assuming hysteresis behavior based on the coherent rotation model. Therefore, the values of coercive fields found in the magnetization loops along or close to the magnetization easy axis cannot be used to predict the anisotropy fields on the basis of the coherent rotational model since they are usually determined by domain nucleation and wall motion. However, as discussed in the following, this model provides a satisfactory account of the angular variation of M_r/M_s.

3.2 Dynamic magnetic properties The dynamic magnetic properties were scrutinized with the help of a previously described MS-FMR [18, 19] setup. The resonance frequencies are obtained from a fit assuming a lorentzian derivative shape of the recorded spectra.

As in Ref. [18], we assume a magnetic energy density which, in addition to Zeeman, demagnetizing and exchange terms, is characterized by the following anisotropy contribution:

$$E_{\text{anis}} = K_\perp \sin^2\theta_M - \frac{1}{2}\left(1 + \cos 2(\varphi_M - \varphi_u)\right) K_u \sin^2\theta_M - \frac{1}{8}\left(3 + \cos 4(\varphi_M - \varphi_4)\right) K_4 \sin^4\theta_M. \quad (1)$$

In the above expression, θ_M and φ_M, respectively, represent the out-of-plane and the in-plane (referring to the

c-axis of the substrate) angles defining the direction of the magnetization M_s; φ_u and φ_4 stand for the angles of the easy uniaxial axis and of the easy fourfold axis, respectively, with this c-axis. With these definitions K_u and K_4 are necessarily positive. As in Ref. [18], it is convenient to introduce the effective magnetization $4\pi M_{eff} = 4\pi M_s - 2K_\perp/M_s$, the uniaxial in-plane anisotropy field $H_u = 2K_u/M_s$ and the fourfold in-plane anisotropy field $H_4 = 4K_4/M_s$.

For an in-plane applied magnetic field H, the studied model provides the following expression of the frequencies of the experimentally observable magnetic modes:

$$F_n^2 = \left(\frac{\gamma}{2\pi}\right)^2 \left[H\cos(\varphi_H - \varphi_M) + \frac{H_4}{2}\cos 4(\varphi_M - \varphi_4) + H_u \cos 2(\varphi_M - \varphi_u) + \frac{2A_{ex}}{M_s}\left(\frac{n\pi}{d}\right)^2 \right] \times \left[H\cos(\varphi_H - \varphi_M) + 4\pi M_{eff} + \frac{H_4}{8}(3 + \cos 4(\varphi_M - \varphi_4)) + \frac{H_u}{2}(1 + \cos 2(\varphi_M - \varphi_u)) + \frac{2A_{ex}}{M_s}\left(\frac{n\pi}{d}\right)^2 \right]. \quad (2)$$

For H normal to the sample plane, large magnetic fields are applied (enough to allow for $M_s//H$) and thus the magnetic in-plane anisotropies can be neglected. Therefore the frequency linearly varies with H as

$$F_\perp = \left(\frac{\gamma}{2\pi}\right)\left[H - 4\pi M_{eff} + \frac{2A_{ex}}{M_s}\left(\frac{n\pi}{d}\right)^2\right]. \quad (3)$$

In the above expressions the gyromagnetic factor γ is related to the effective Landé factor g through: $(\gamma/2\pi) = g \times 1.397 \times 10^6$ Hz/Oe. The uniform mode corresponds to $n = 0$. The other modes to be considered (perpendicular standing spin waves, PSSW) are connected to integer values of n: their frequencies depend upon the exchange stiffness constant A_{ex} and upon the film thickness d.

For all the films the magnetic parameters at room temperature were derived from our MS-FMR measurements.

3.2.1 Gyromagnetic *g*-factor, magnetization, and exchange stiffness In perpendicular configuration the MS-FMR technique allows for deriving the values of g and of $4\pi M_{eff}$ from the variation of the resonance frequency *versus* the magnitude of the applied field using Eq. (3). The MS-FMR field dependences of the resonance frequencies of the uniform and of the PSSW modes are shown in Fig. 3 for the 50- and the 100-nm-thick samples. The frequencies vary linearly with H. The PSSW mode shows a frequency higher than the uniform one, by an amount independent of H, as expected from the studied model. The derived value of g is independent of the sample $g = 2.04$. It is in good agreement with previous determinations [15]. The effective demagnetizing field $4\pi M_{eff}$ slightly increases *versus* the sample thickness but remains close to the saturation magnetization (12,200 Oe) given by Hamrle et al. [21]: it is reported in Table 1.

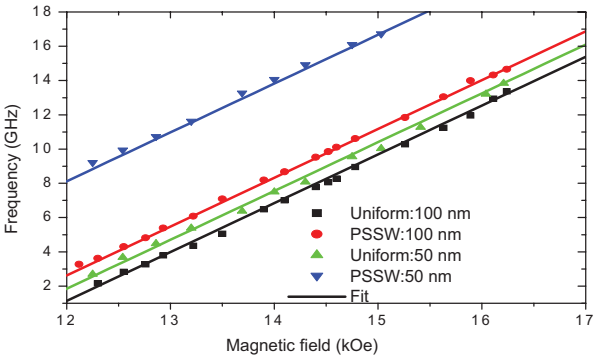

Figure 3 (online color at: www.pss-a.com) Field dependence of the resonance frequency of the uniform precession and of the first perpendicular standing spin wave excited (PSSW) mode of 50- and 100-nm thick films. The magnetic field is applied perpendicular to the film plane. The fits are obtained using Eq. (3) with the parameters indicated in Table 1.

3.2.2 In-plane anisotropies Figures 4b, d, and f illustrate the experimental in-plane angular dependence of the frequency of the uniform mode in the 20-, 50-, and 100-nm-thick films, compared to the obtained fits using Eq. (2). For all the samples, the obtained values of the magnetic parameters corresponding to the best fits are reported in Table 1. In all the investigated films the c-axis of the substrate coincides with a principal direction of the fourfold magnetic anisotropy: it defines a hard axis ($\varphi_4 = 45°$) except, surprisingly, in the 50-nm sample for which it defines an easy axis ($\varphi_4 = 0°$). The directions of the principal axes of the twofold anisotropy are sample dependent. The observed variations of the in-plane magnetic anisotropy are not clearly related either to the thickness or to the crystallographic texture (which does not significantly change). During the preparation of the films uncontrolled parameters presumably

Table 1 Magnetic parameters obtained from the best fits to our experimental results.

thickness (nm)	A_{ex} (μerg/cm)	$4\pi M_{eff}$ (kOe)	$H_u = 2K_u/M_s$ (Oe)	$H_4 = 4K_4/M_s$ (Oe)	φ_u (°)	φ_4 (°)
20	n.m.[a]	11	20	72	0	45
50	2.87	11.35	26	88	−13	0
100	2.56	11.6	16	48	0	45

φ_u and φ_4 are the angles of the in-plane uniaxial and of the fourfold anisotropy easy axes, respectively.
[a]Not measured.

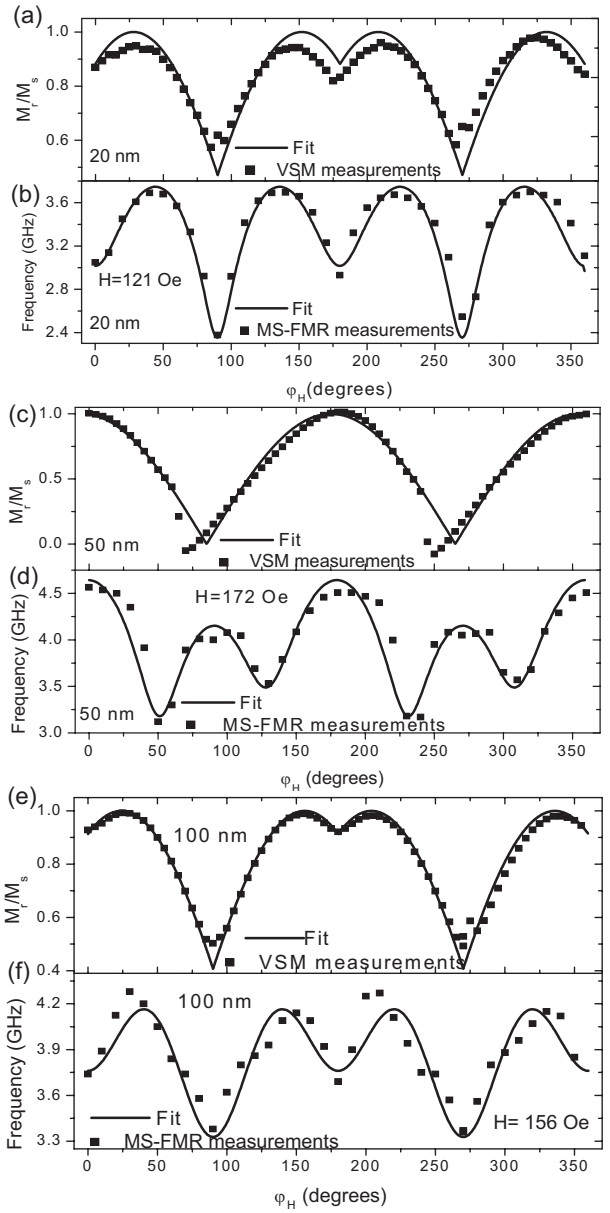

Figure 4 Reduced remanent magnetization of the (a) 20-nm, (c) 50-nm, and (e) 100-nm-thick Co_2MnSi films. The full lines are obtained from the energy minimization using the parameters reported in Table 1. (b), (d), and (f) show the compared in-plane angular dependences of the resonance frequency of the uniform modes. The fit is obtained using Eq. (2) with the parameters indicated in Table 1.

induce different stress conditions giving rise to changes in the magnetic anisotropy. Therefore, we think that this difference and change in the anisotropy axes between the different samples maybe due to the different local stress, sample process, growth condition, and to the complex film structure. It is not possible to derive a quantitative understanding of the anisotropies resulting from the real film structure. However, we should mention that we measure effective anisotropies averaged over the entire sample volume which is structurally strongly non-uniform and thickness dependent. Assuming that the local anisotropies are intimately connected with the local orientation of the crystal axes which strongly varies between the six different domains a simple or unique character of the magnetic anisotropy cannot be expected.

Finally, it is interesting to notice that the set of in-plane magnetic anisotropy parameters deduced from the in-plane angular dependence of the magnetic resonance for the 20-, 50-, and 100-nm-thick samples allows for a good fit of the angular variation of the normalized static remanence calculated with the help of the coherent rotation model, as shown in Fig. 4. This variation only depends on φ_u, φ_4, and H_u/H_4.

It results from the present study and from our previous ones [18, 19] that the growth of Heusler thin films on sapphire substrates is complex and depends on the conditions of the sample preparation. Therefore the magnetic properties cannot be tuned rigorously.

4 Conclusion Co_2MnSi films of thicknesses varying from 20, 50, and 100 nm were prepared by sputtering on *a*-plane sapphire substrates. They show practically identical crystallographic textures, as revealed by our X-rays diffraction studies, with a cubic [110] axis normal to the film-plane and with a well defined manifold of in-plane orientations referring to the *c*-axis of the substrate. The microstrip ferromagnetic resonance gives access to effective g factors which do not differ from each other and to effective demagnetizing fields which are close to the magnetization at saturation and which slightly increase with the sample thickness. In addition, this technique allowed us for evaluating the exchange stiffness constant which, as expected, was found not to significantly depend on the studied sample. The in-plane anisotropy was investigated through the study of the dependence of the resonance frequency *versus* the orientation of an in-plane applied magnetic field: it presents two contributions, showing a fourfold and a twofold axial symmetry, respectively. A principal fourfold axis parallel to *c* is always found, but it can be the easy or the hard axis. Depending on the studied film the twofold axes can be misaligned with the fourfold ones. The angular dependence of the remanent normalized magnetization, studied by VSM and analyzed within the frame of a coherent rotation model, is in agreement with these conclusions. The general magnetic behavior is similar to the previously published one observed in Heusler Co_2MnGe films [18, 19]. Apparently, there is no simple relation between the observed dispersion of the in-plane anisotropy parameters and the thickness or the crystallographic texture of the samples.

References

[1] R. J. Soulen, Jr., J. M. Byers, M. S. Osofsky, B. Nadgorny, T. Ambrose, S. F. Cheng, P. R. Broussard, C. T. Tanaks, J. Nowak, J. S. Moodera, A. Barry, and J. M. D. Coey, Science **282**, 85 (1998).

[2] P. J. Webster, J. Phys. Chem. Solids **32**, 1221 (1971).

[3] J. Schmalhorst, S. Kämmerer, M. Sacher, G. Reiss, A. Hütten, and A. Scholl, Phys. Rev. B **70**, 024426 (2004).
[4] Y. Sakuraba, J. Nakata, M. Oogane, H. Kubota, Y. Ando, A. Sakuma, and T. Miyazaki, Jpn. J. Appl. Phys. **44**, L1100 (2005).
[5] M. Oogane, Y. Sakuraba, J. Nakata, H. Kubota, Y. Ando, A. Sakuma, and T. Miyazaki, J. Phys. D: Appl. Phys. **39**, 834 (2006).
[6] Y. Sakuraba, M. Hattori, M. Oogane, Y. Ando, H. Kato, A. Sakuma, T. Miyazaki, and H. Kubota, Appl. Phys. Lett. **88**, 192508 (2006).
[7] K. Inomata, N. Ikeda, N. Tezuka, R. Goto, S. Sugimoto, M. Wojcik, and E. Jedryka, Sci. Technol. Adv. Mater. **9**, 014101 (2008).
[8] T. Ishikawa, S. Hakamata, K. Matsuda, T. Uemura, and M. Yamamoto, J. Appl. Phys. **103**, 07A919 (02008).
[9] C. T. Tanaka, J. Nowak, and J. S. Moodera, J. Appl. Phys. **86**, 6239 (1999).
[10] S. Kämmerer, A. Thomas, A. Hütten, and G. Reiss, Appl. Phys. Lett. **85**, 79 (2004).
[11] A. Conca, S. Falk, G. Jakob, M. Jourdan, and H. Adrian, J. Magn. Magn. Mater. **290/291**, 1127 (2004).
[12] H. Kubota, J. Nakata, M. Oogane, Y. Ando, A. Sakumam, and T. Miyazaki, Jpn. J. Appl. Phys. **43**, L984 (2004).
[13] S. Tsunegi, Y. Sakuraba, M. Oogane, K. Takanashi, and Y. Ando, Appl. Phys. Lett. **93**, 112506 (2008).
[14] Y. Liu, L. R. Shelford, V. V. Kruglyak, R. J. Hicken, Y. Sakuraba, M. Oogane, and Y. Ando, Phys. Rev. B **81**, 094402 (2010).
[15] B. Rameev, F. Yildiz, S. Kazan, B. Aktas, A. Gupta, L. R. Tagirov, D. Rata, D. Buergler, P. Gruenberg, C. M. Schneider, S. Kämmerer, G. Reiss, and A. Hütten, Phys. Status Solidi A **203**, 1503 (2006).
[16] R. Yilgin, M. Oogane, Y. Ando, and T. Miyazaki, J. Magn. Magn. Mater. **310**, 2322 (2007).
[17] O. Gaier, J. Hamrle, S. J. Hermsdoerfer, H. Schultheiß, B. Hillebrands, Y. Sakuraba, M. Oogane, and Y. Ando, J. Appl. Phys. **103**, 103910 (2008).
[18] M. Belmeguenai, F. Zighem, Y. Roussigné, S.-M. Chérif, P. Moch, K. Westerholt, G. Woltersdorf, and G. Bayreuther, Phys. Rev. B **79**, 024419 (2009).
[19] M. Belmeguenai, F. Zighem, T. Chauveau, D. Faurie, Y. Roussigné, S.-M. Chérif, P. Moch, K. Westerholt, and P. Monod, J. Appl. Phys. **108**, 063926 (2010).
[20] U. Geiersbach, A. Bergmann, and K. Westerholt, J. Magn. Magn. Mater. **240**, 546 (2002).
[21] J. Hamrle, O. Gaier, S.-Gi. Min, B. Hillebrands, Y. Sakuraba, and Y. Ando, J. Phys. D: Appl. Phys. **42**, 084005 (2009).